

2023

Characterization of the subcellular structure of engineered cardiomyocytes using small angle X-ray scattering

<https://hdl.handle.net/2144/45447>

"Downloaded from OpenBU. Boston University's institutional repository."

BOSTON UNIVERSITY
COLLEGE OF ENGINEERING

Thesis

**CHARACTERIZATION OF THE SUBCELLULAR STRUCTURE
OF ENGINEERED CARDIOMYOCYTES USING
SMALL ANGLE X-RAY SCATTERING**

by

GEOFFREY ROBERT VAN DOVER

B.A., St. Olaf College, 2020

Submitted in partial fulfillment of the
requirements for the degree of
Master of Science

2023

© 2023 by
GEOFFREY ROBERT VAN DOVER
All rights reserved

Approved by

First Reader

David J. Bishop, Ph.D.
Professor of Electrical and Computer Engineering
Professor of Physics
Professor and Division Head of Materials Science and Engineering
Professor of Mechanical Engineering
Professor of Biomedical Engineering

Second Reader

Christopher Chen, M.D., Ph.D.
William Fairfield Warren Distinguished Professor
Professor of Biomedical Engineering
Professor of Materials Science and Engineering

Acknowledgements

I would like to acknowledge Dr. Josh Javor for his initial contributions to this project including data collection and his guidance throughout this research. I would also like to thank Dr. Christopher Chen and his graduate student Jourdan Ewoldt as well as Joshua Lee for providing the tissue samples and for overall contributions to this project. I would like to thank Misha Zhernenkov, Guillaume Freychet, and Patryk Wasik for their work and expertise at the synchrotron at Brookhaven National Laboratory. And finally, I want to acknowledge my research advisor, Professor David Bishop, for his support throughout my Master's Thesis program.

**CHARACTERIZATION OF THE SUBCELLULAR STRUCTURE
OF ENGINEERED CARDIOMYOCYTES USING
SMALL ANGLE X-RAY SCATTERING
GEOFFREY ROBERT VAN DOVER**

ABSTRACT

The structural and functional development of human induced pluripotent stem cell-derived cardiomyocytes (hiPSC-CMs) is essential to understand in order to enable pharmaceutical testing, disease modeling, and ultimately therapeutic use. Recent developments in the field of bioengineering have led to improvements in the efficiency and efficacy of growth methods that allow hiPSC-CMs to be studied in greater detail. However, engineered cardiac tissue still has not achieved a level of maturation necessary for the majority of biomedical applications. Thus, new technologies and methods are necessary to realize the long-term benefits of engineered cardiac tissue. To better understand the development of the tissue, further characterization of the structure and function of these cardiomyocytes is required. In this work, we describe advances using a method not commonly applied to these materials, Small Angle X-ray Scattering (SAXS). SAXS was used to characterize the structural development of hiPSC-CMs on a 3D multicellular platform in their early stages of maturation.

The myofilament lattice spacing was found to monotonically decrease as the tissue matured from its initial state post-seeding at a rate between 0.75 and 1 nm per day between days 3 and 10 of maturation. With 49 total samples across three different batches of tissue, the p value for correlation between the lattice plane spacing and maturation time was $p < 0.05$, indicating a statistically significant correlation.

In tests of the tissue response to fixation with varying doses of KCl relaxation buffer, results showed a general trend of decreased myofilament spacing with increasing KCl concentration. However, in the concentrations between 60mM and 120mM, a characteristic increase in spacing is observed.

Beat force was also measured prior to measuring myofilament spacing and this resulted in a graphically suggestive correlation. However, ANOVA analysis results in a p value of 0.35 which is statistically insignificant.

Finally, methods were tested to monitor the myofilament lattice spacing in contracting tissue and found no evidence of contraction-based changes in the myofilament lattice.

<u>Table of Contents:</u>	Page
Acknowledgements	iv
Abstract	v
Table of Contents	vii
List of Figures	ix
1. Introduction	1
1.1 General Background	1
1.2 The Myosin Filament	2
1.3 Frank-Starling Law	4
1.4 Tissue Imaging Methods	6
1.5 Small Angle X-ray Scattering	10
1.6 SAXS as A Method of Structural Analysis of Cardiac Tissue	13
1.7 Objectives	15
1.8 Hypothesis	16
2 Methods and Materials	17
2.1 Tissue Cultivation	17
2.2 Tissue Fixation	19
2.3 Sample Preparation for Synchrotron	20
2.4 SAXS Setup for Tissue Measurement	22

2.5	Data Acquisition.....	22
2.6	SAXS Data Python/MATLAB Processing and Analysis.....	24
3	Results	27
3.1	Variance based on Acquisition Method.....	27
3.2	Colormaps of Measurements	29
3.3	Myofilament Spacing vs. Maturation Time.....	30
3.4	Myofilament vs. Relaxation Buffer Concentration.....	34
3.5	Myofilament Spacing vs. Contractility.....	37
3.6	SAXS Live Tests.....	38
4	Discussion.....	40
4.1	Spacing of the Myofilament lattice	40
4.2	Effect of Relaxation Buffer on the D-Spacing.....	43
4.3	Contractility of hiPSC-CMs	44
4.4	Contraction Tests	46
5	Conclusion	48
	Bibliography.....	50
	Vita	54

List of Figures

	Page
Figure 1: Myosin and Actin filaments in muscle tissue ⁷	3
Figure 2: Simple model of the Frank-Starling Law ⁹	5
Figure 3: Image result of TPEF analysis of rat cardiac tissue ¹³	8
Figure 4: Ultrastructure of cardiomyocyte under TEM ¹⁵	10
Figure 5: SAXS method of scattering for measurement of a protein in buffer ¹⁷	12
Figure 6: (a) Standard image result of SAXS measurement. (b) plot of data post azimuthal integration ¹⁶	13
Figure 7: Design of the PDMS well the tissue is seeded in. [created by Josh Javor].....	19
Figure 8: (a) Cardiac microtissue on pillars in Kapton-glass chamber. (b) Standard image result of x-ray diffraction ¹⁹	22
Figure 9: (a) Tissue orientation to SAXS beam and size of SAXS beam. (b) Standard TIF image result of SAXS measurement. (c) cardiomyocyte myoactin nanostructure ¹⁹	24
Figure 10: Visual of the 1,0 and 1,1 planes in the myo-actin complex ¹⁹	26
Figure 11: (A) Three tested methods for data collection in samples. (B) Plot of standard deviation of spacing of samples by number of points averaged [created by Josh Javor].....	28

Figure 12: (a) Interpolated colormaps of the myofilament spacing in the tissue	
(b) Visual of location of SAXS measurements on tissue [created by Josh Javor]
30
Figure 13: (A) d-spacing of myofilament vs. maturation time for batches 1–332
Figure 14: d-spacing of myofilament vs. maturation time for HCM tissue34
Figure 15: Myofilament d-spacing vs. concentration of KCl buffer for batches	
1(A) and 3 (B)36
Figure 16: Beat force vs. myofilament spacing for batches 1 (A) and 3 (B)37
Figure 17: Movement of pillar that monitors contraction frequency and beat	
force in live tissue39
Figure 18: Change in myofilament spacing over time of contraction39

1 Introduction

1.1 General background

The leading cause of death in the world is cardiovascular disease.¹ The most common genetic cardiovascular disease is hypertrophic cardiomyopathy (HCM), a genetic mutation that leads to a variety of phenotypical expressions, but most notably causes the heart muscle to thicken, making it more difficult for the heart to pump blood and ultimately leading to heart failure. While drug therapies and lifestyle changes can be beneficial to a patient, there is no current cure for cardiovascular disease.

There have been many significant advancements in the field of cardiac tissue engineering over the last decade². Improvements in the methods of cultivation of human induced pluripotent stem cell-derived cardiomyocytes (hiPSC-CM) have resulted in the advancement of 3D stem cell cultures with increased cell growth, organization, and structural and functional maturation. Customized 3D environments have been shown to improve the maturation of these tissue matrices in terms of cell morphology, contractility, and organization of the myofibrils². The development of functional hiPSC-CM matrices has far-reaching effects in the fields of disease modeling, pharmaceutical testing, and therapeutics

with the ultimate promise of the use of these tissue cultures for organ repair.

Despite advancements, hiPSC-CMs are not currently capable of mimicking the structure and function of matured human heart tissue. At present, hiPSC-CMs produce beat forces tenfold smaller than human tissue³. Studies on the anisotropy of this bioengineered tissue also show a level of organization significantly lower than human tissue. These characteristics are results of the subcellular structure of developing hiPSC-CMs. Subcellular techniques have been developed to probe function, with readouts such as action potential⁴, traction force, and metabolism⁵, but most of these techniques are limited to 2D and surface readouts. While these measurements provide vital information, unlike 3D measurements, they lack an ability to encompass the entire tissue, which is necessary for the characterization of the structure of a cell.

1.2 The Myosin Filament

The smallest subunit of the cardiomyocyte is the sarcomere. In the sarcomere are a series of alternating thick and thin protein filaments that slide past each other and are responsible for the mechanism of muscle contraction via electromechanical coupling and the transmission of neurotransmitters. These

filaments are the myosin (thick) and actin (thin) fibers (Figure 1). The myosin filament has a long tail with a head that binds to the actin filament in the presence of $[Ca^{2+}]$. Changes in conformation of this myosin head cause the actin filament to slide along the myofibril; i.e., a contraction. A difference in this subcellular structure can have significant effects on the dynamics of contraction of the muscle tissue. A longer sarcomere length will increase the number of interacting crossbridges between the two filaments and a change in the filament spacing can increase or decrease the crossbridge density⁶. However, the implications that these structural changes have on the function and performance of the tissue is not well understood.

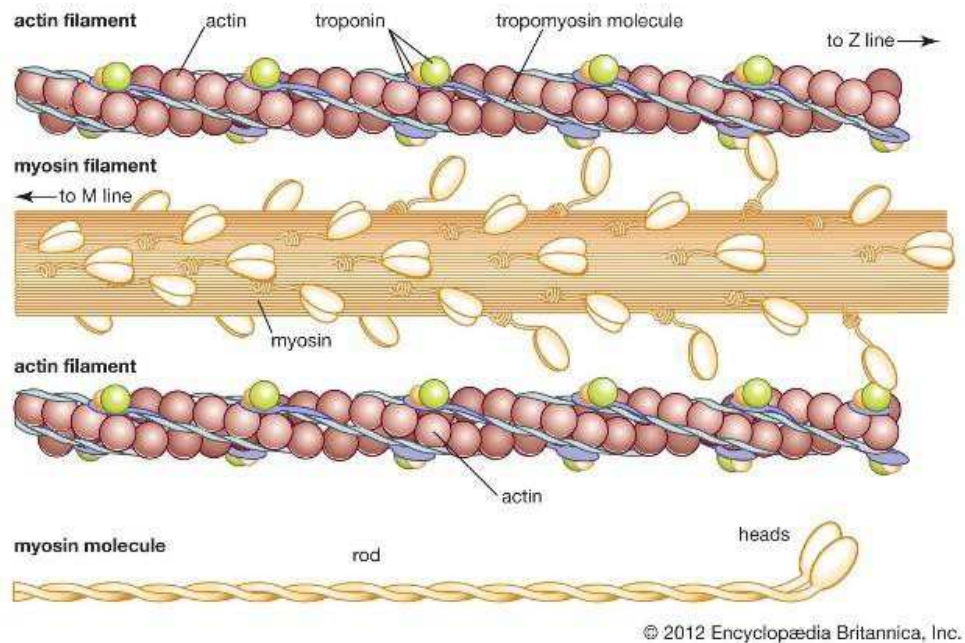


Figure 1: Myosin and Actin filaments in muscle tissue.⁷

1.3 Frank-Starling Law

In nature, structure dictates function. In biology, this remains the case; however, the relationship between the two can be ambiguous. A perfect example of this is the mystery of the Frank-Starling relationship (Figure 2), which captures an intrinsic property of cardiomyocytes: increased sarcomeric length (or ventricular volume) results in increased contractility⁶. The increased ventricular volume accommodates a greater venous return and thus allows for a greater stroke volume during contraction. Therefore, a greater volume of blood is ejected from the heart. With this change in structure, the performance of the tissue is enhanced. However, this explanation for increased performance with sarcomere length is one of many possible mechanisms of the Frank-Starling relationship.

Another hypothesis for this same structural change is that with longer sarcomere length, more crossbridges interact with the actin filament due to a change in the lateral spacing of the thick and thin (myosin and actin) filaments. With more crossbridge interactions, there are more active myosin heads to change in conformation, resulting in a greater contractile force⁶. Studies in permeabilized myocardium of consistent length illustrate that the same changes in contractile force can be achieved with changes in the fiber diameter and with increased presence of Ca^{2+} .⁸ However, these studies have only measured muscle

diameter and not the lateral spacing between the thick and thin filaments. Determining the lateral spacing between the thick and thin filaments would provide insight into the mechanisms that underlie the Frank-Starling relation.

The Frank-Starling law tells us that function is tightly connected to structure, but not in a way that we fully understand. To define this relationship better, studies must characterize the subcellular structure of functional tissue and then connect this to functional measurements.

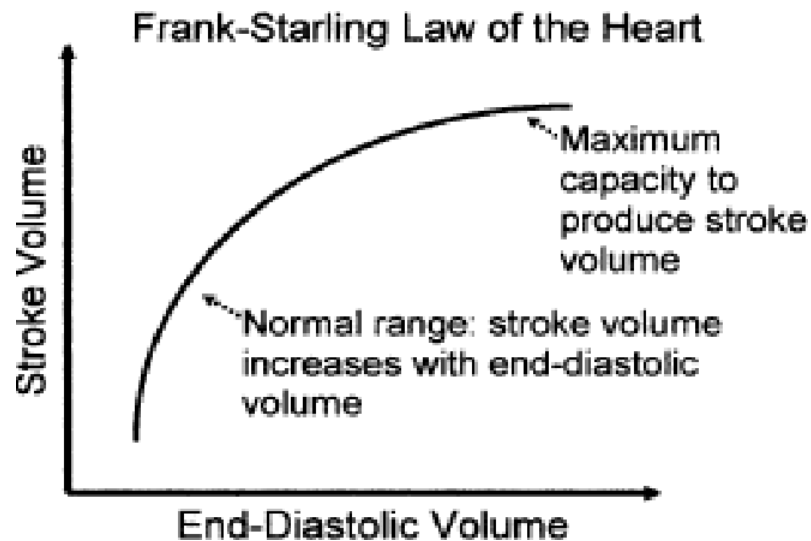


Figure 2: Simple model of the Frank-Starling Law showcasing relationship between sarcomere length (ventricular volume) and stroke volume.⁹

1.4 Tissue Imaging Methods

Detailed and thorough examination of both the structure and functional properties of tissue are essential to understand the underlying relationship. Biologists have spent decades improving existing methods of characterization and developing new ones. Biologists first developed optical microscopy which was closely followed by its counterpart, fluorescence microscopy. To circumvent the limitations of optical microscopy, electron microscopy (EM) was developed. While EM surpasses optical microscopy in terms of resolution, it suffers from its own drawbacks. From this, biologists have turned to x-ray diffraction for even greater compatibility.

Optical microscopy is a core technology for biological measurements. Optical microscopy imaging covers the basic compound microscope, fluorescence imaging, and two photon excitation microscopy. Used in every biological lab, optical microscopy has the advantages of being relatively easy to use, inexpensive, and capable of resolution on the scale of $0.1\mu\text{m}$.¹⁰ Because the standard cell diameter is in the range of $1\text{-}100\mu\text{m}$, optical microscopy is ideal for the examination of cell matrices, though it is inadequate for the visualization of single cells due to a lack of resolution at this scale. When paired with staining techniques however, optical microscopy is capable of highlighting certain

organelles and ascertaining superficial measurements of cellular structure such as size, shape, and extracellular space; i.e., important aspects of cellular organization¹¹. Due to a lack of resolution, most forms of optical microscopy are not capable of the direct detection of the subcellular structure¹².

Two photon excitation microscopy (TPEF) is a sophisticated method of optical microscopy. A subcategory of fluorescence imaging, TPEF utilizes the excitation of a fluorescent moiety by two photons with energies half of the energy needed to excite fluorescence¹². The usage of this low energy, long wavelength near-infrared excitation light minimizes scattering in the tissue while the multiphoton absorption boosts the signal. The combination of these two aspects of TPEF lead to deeper tissue penetration, efficient light detection, and reduced photobleaching. In 2010, Bub and Camelliti showed that TPEF is capable of highly resolved visualization of sarcomere length in Langendorff-perfused rat cardiomyocytes, both in situ and in vitro. Figure 3 shows the image results obtained from TPEF of tissue stained with di-4-ANEPPS, a voltage sensitive dye that stains T-tubules. In the resting heart cells, the mode of the distribution of sarcomere lengths was found to be $1.95 \mu\text{m}$ ¹³. This study showed the capabilities of TPEF to characterize the subcellular structure of cardiomyocytes on the micrometer scale. However, in general optical microscopy requires

demembration of the cell for proper resolution due to a low depth penetration.

This is a method that can significantly affect the structure of the sample.

Furthermore, the capabilities of optical microscopy stop at the micrometer scale. Greater spatial resolution is required for the characterization of cellular structures smaller than the sarcomere. Specifically, characterizing the thick and thin filaments requires imaging capable of resolution on the nanometer scale.

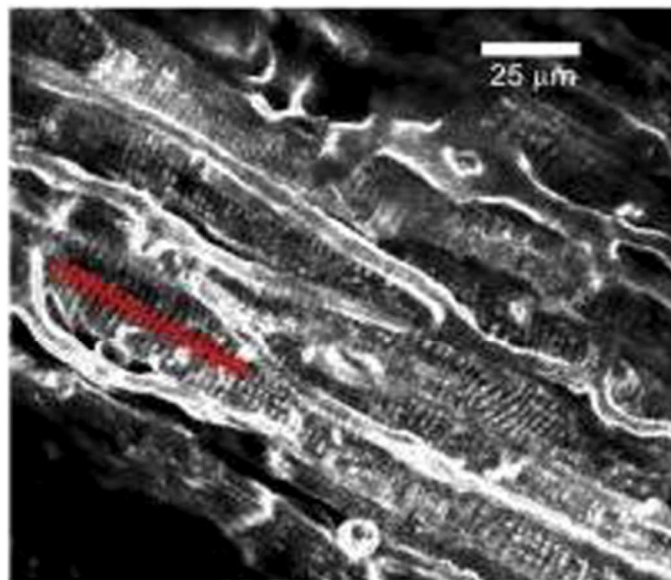


Figure 3: Image result of TPEF analysis of Langendorff rat cardiomyocytes¹³.

Electron microscopy (EM) utilizes a beam of accelerated electrons as the probe. In contrast to TPEF, it uses a probe with de Broglie wavelengths up to 100,000 times shorter than visible light¹². This allows for a resolution superior to the light microscope. Cryogenic electron microscopy (Cryo-SEM) and

transmission electron microscopy (Cryo-TEM) are two forms of high-resolution imaging which are able to resolve to 0.4 nm and 0.2 nm respectively. While this resolution capability is ideal for the visualization of nanometer-scale cellular structures, the scattering of electrons restricts the depth of penetration to 1 μ m, reducing the visualization of a multicellular complex to its surface¹⁴. To achieve a 3D analysis, samples are fabricated through cryo-immobilization and desiccation, followed by slicing out small regions with a focused ion beam¹⁰.

While it has not been fully studied, these preparation steps can affect the structure of the sample¹⁰. Although TEM and SEM are capable of visualization of subcellular structures on the nanometer scale, the methods they require as well as their innate limitations mean these imaging methods are suboptimal for the analysis of the structure of functional cardiomyocytes.

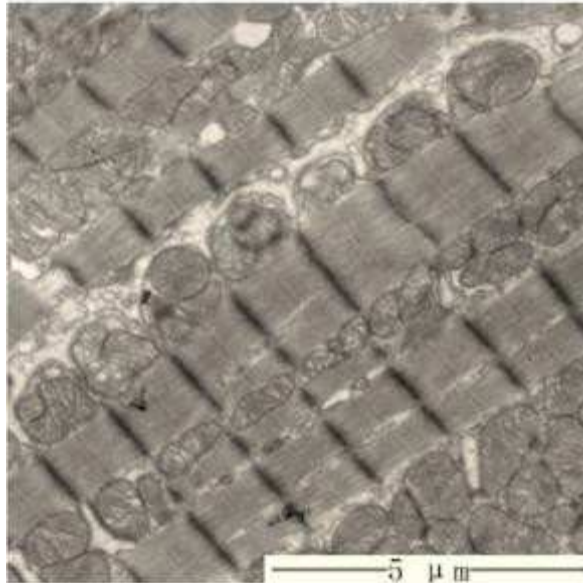


Figure 4: Ultrastructure of cardiomyocyte under TEM¹⁵.

1.5 Small Angle X-ray Scattering

Small angle x-ray scattering (SAXS) is capable of measuring nanoscale structures of a sample. X-ray diffraction can be understood in terms of Bragg's law which relates the angle of scattering of x-rays in a material to a propagation path length difference between diffracting planes, thus providing an unambiguous measurement of the spacing between planes^{16,17}. While most commonly used for crystalline solid-state samples to infer the dimensions of a lattice structure of a material, SAXS has also long been used in the measurement of macromolecules such as proteins as shown in Figure 5. Specifically, SAXS is a

powerful method for resolving the size and shape of these macromolecules, as well as determining pore sizes. Recent advancements in synchrotron technology and noise reduction methods enable SAXS to serve as a valuable imaging method for semi-crystalline materials. Thus, the resolution of SAXS makes it an ideal method for the study of the semi-ordered subcellular structure of biological tissue. While capable of producing these desired high-resolution measurements, SAXS results can be challenging to interpret because samples typically comprise a mixture of random orientations of the target along with the presence of other macromolecules; these contribute to a low signal with large amounts of noise.

Despite this low signal to noise ratio (SNR), the spatial scale of SAXS measurements paired with its affinity to biological samples enables SAXS to be unmatched in the measurement of the myofilament lattice of cardiomyocytes (30-50 nm).

SAXS has no sample preparation steps involving flash freezing, desiccation, or demembration. While it does risk radiation damage to live tissue, SAXS poses no risk for fixed tissue. The photon beam is capable of penetrating through thicknesses exceeding 100 μm , unlike any other high resolution imaging technique. Furthermore, the aforementioned imaging methods are all generally only capable of characterization of a 2D structure of

individual measurements while SAXS measures over an area of a material, allowing for characterization of 3D samples as well as spatial averaging. SAXS is also capable of a much higher collection rate than those imaging methods. This, paired with the high spatial resolution as well as non-violent tissue preparation, makes SAXS ideal for the study of the myofilament lattice spacing in both fixed and live cardiac tissue.

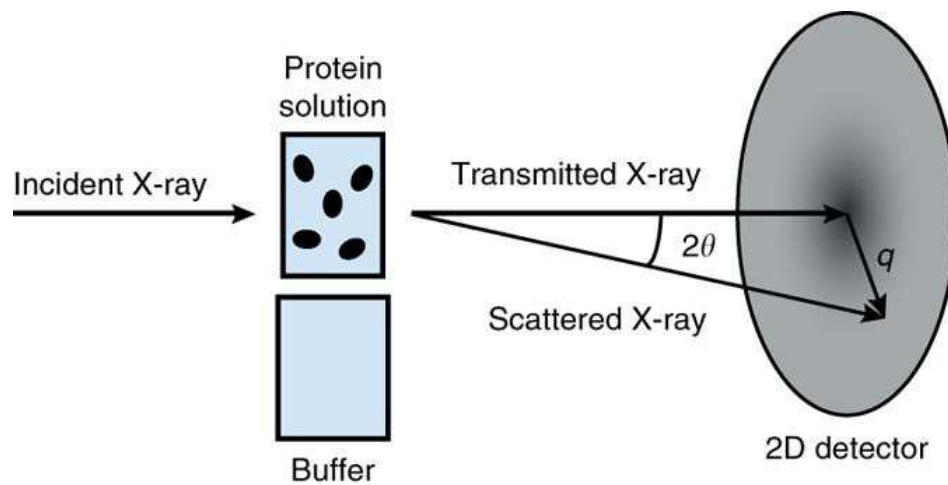


Figure 5: SAXS method of scattering for measurement of a protein in buffer¹⁷.

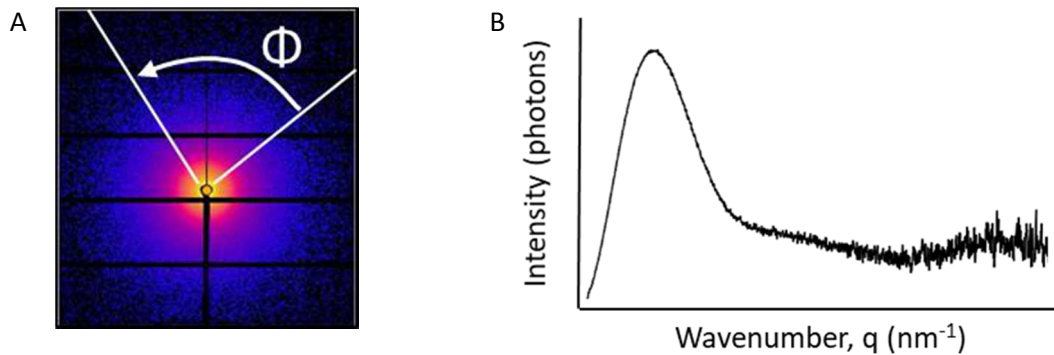


Figure 6: (a) Standard image result of SAXS measurement. (b) Image information is azimuthally integrated ($q=4\pi\sin(\theta)/\lambda$, $I=q^{-c+d}$). Integration results are often illustrated by Guinier and Kratky plots¹⁶.

1.6 SAXS as a Method for Structural Analysis of Cardiac Tissue

The capabilities of SAXS in the characterization of the nanostructure of cardiomyocytes has been showcased in a study done by Brunello et al. on the dynamics of contraction in cardiac tissue¹⁸. In this study, researchers used x-ray diffraction to detect a semi-ordered system in excised rat cardiac tissue. Analysis of the signal from the diffraction of the x-rays allowed the researchers to characterize the crossbridge density of the myosin heads, the conformation of the myosin heads during contraction, and thus an aspect of the nanostructure of the thick and thin filaments. Thorough characterization of this nanostructure is not possible using optical or electron microscopy.

The usage of SAXS for the study of the cardiomyocyte's nanostructure has flourished in the last decade, SAXS can now be used to measure structural changes in live tissue during contraction¹⁸. The signals from different aspects of the sarcomeres structure have been identified, analyzed, and characterized. The SAXS signal resulting from the spacing of the myofilament lattice has been identified and has been studied specifically in rat tissue and matured human tissue. However, hiPSC-CMs are not as matured as adult tissue and therefore may show significant structural evolution. The structural differences between hiPSC-CMs and adult heart tissue has not been studied. In 2020, Javor et. al showed that the myofilament lattice in bioengineered cardiac tissue is a semi-ordered system and is detectable using SAXS. The spacing of the myofilament lattice in these cardiomyocytes was found to be approximately 44 nm¹⁹. This is distinct from measurements in adult heart tissue, which found the spacing to average 39 nm²⁰. The resolution available in the SAXS technique, along with advances in background suppression and subtraction, and spatial averaging have enabled SAXS to serve as a particularly effective method to study the myofilament structure of bio-engineered cardiac tissue.

1.7 Objectives

SAXS enables unique insights into the structure of biological tissue. A substantial amount of information about the nanostructure of cardiomyocytes has been accumulated from SAXS studies done on cardiac tissue from humans, rats, and zebrafish¹⁸⁻²⁰. The information gathered from these studies has proved invaluable in developing an understanding of the relation between structure and function. While some studies have even been able to monitor changes in the structure during induced contractions¹⁸, no SAXS study on bio-engineered human cardiomyocytes has monitored a natural heartbeat.

There is little information regarding the structure of immature, bioengineered tissue. Characterizing the nanostructure of immature, multicellular systems can provide critical information that can improve cultivation methods and bridge the gap between bioengineered tissue and natural heart tissue. In order to better understand this relationship between structure and function, thorough characterization of the nanostructure of engineered tissue is needed to create a baseline for comparison in the analysis of the myofilament lattice's evolution. The present study will characterize the development of the spacing of the myofilament lattice in bio-engineered hiPSC-

CMs in the early stages of maturation. Additionally, this work aims to develop and optimize methods used for SAXS measurement of engineered tissue, including the fixation process, the amount of time the tissue is given to mature, the transition process from cultivation to SAXS measurement, and the methods and parameters associated with SAXS measurement and data analysis *per se*. Finally, this work reflects on efforts to monitor live contracting tissue without the use of external manipulators.

1.8 Hypothesis

In this study of the development of the structure of multicellular hiPSC-CM systems, the nanostructure, specifically the spacing of the myofilament lattice, will vary depending on numerous factors, including maturation time, exposure to KCl, height and position within the cellular matrix and, importantly, genetic mutations present within the cardiomyocytes.

2 Materials and Methods

2.1 Tissue Cultivation

To cultivate and measure hiPSC-derived cardiomyocytes (CMs), hiPSCs from the PGP1 parent line and CRISPR-cas9 PGP1-edited cells with a heterozygous R403Q+ mutation in the β -myosin heavy chain (MYH7) were received from the Seidman Lab²¹. The hiPSCs were kept in mTeSR1, a standard stem cell culture medium (StemCell) on Matrigel, an ECM matrix-mimicking hydrogel (Fisher), that was mixed at a ratio of 1:80 in DEMEM/F-12, a basal media (Fisher). The mixture was then split at a confluence of 60–90% with Accutase (Fisher). The stem cells were differentiated into cardiomyocytes through small molecule, monolayer-based manipulation of the Wnt signaling pathway²². When contractions were observed in the cells, the cardiomyocytes were purified over 2–5 days with RPMI no-glucose media (Fisher) and 4mM sodium DL lactate μ solution (Sigma). Post-selection, CMs were replated and maintained in RPMI with 1:50 B-27 Supplement (Fisher) on 10 μ g/mL fibronectin (Fisher)-coated plates until day 30+.

A previous design of cardiac micro-tissue (CMT) devices with tissue wells was used for the cultivation of the CMTs²³. These devices are equipped with two micropillars with spherical caps designed to suspend the tissue matrix. The

devices were cast in polydimethylsiloxane (PDMS) using a 3D printed mold (Protolabs). They were then plasma treated for 60s, treated for 2h with 0.01% Poly-L-Lysine (PLL) (ScienCell) and 15 min with 0.1% glutaraldehyde (EMS), before being washed 3x with DI water. They were then allowed to sit at 4°C overnight. Before seeding, the devices were washed with 70% ethanol for 30 min, dried, and UV-sterilized for 15 min. 2 μ L of 2% Pluronic F-127 surfactant (Sigma) was added to each well and incubated at RT for 30 min to prevent the CMTs from adhering to the bottom surface of the wells.

Each CMT has roughly 60,000 cells, comprising 90% iPSC-CMs and 10% normal human ventricular cardiac fibroblasts (NHCF-V). The CMTs were mixed in 7.5 μ L of an extracellular matrix solution: 4mg/mL human fibrinogen (Sigma), 10% Matrigel (Corning), 1.6 mg/mL thrombin (Sigma), 5 μ M Y-27632 a selective kinase inhibitor (Tocris), and 33 μ g/mL aprotinin (Sigma). This mixture was pipetted into the devices, polymerized for 5 min, and afterwards a growth media was added and replaced every other day. This growth media contained: high- glucose DMEM (Fisher) with 10% fetal bovine serum (Sigma), 1% penicillin-streptomycin (Fisher), 1% nonessential amino acids (Fisher), 1% GlutaMAX (Fisher), 5 μ M Y-27632, and 33 μ g/mL aprotinin. The Y-27632 was removed 2 days after seeding, and after 7 days the aprotinin was decreased to 16 μ g/mL. Tissues

were maintained/matured in an incubator at 37°C and 5% CO₂ for between 3 and 10 days.

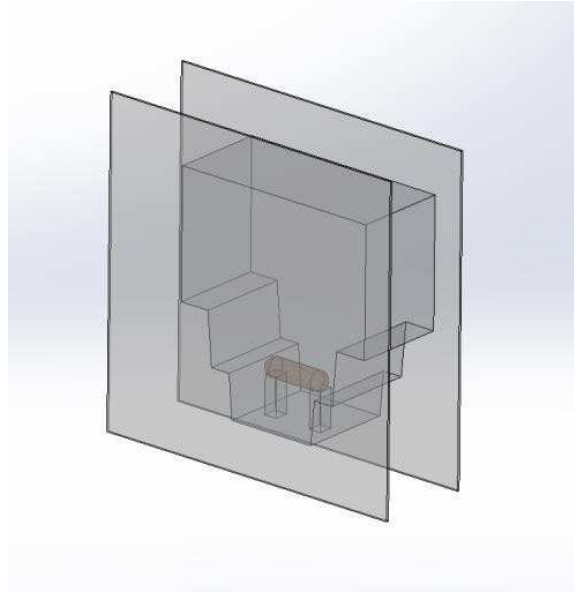


Figure 7: Design of the PDMS well the tissue is seeded in.

2.2 Tissue Fixation

After the chosen maturation time and after biological measurements, CMTs were submerged 30 min in 4% PFA (Fisher), washed in PBS, and stored in PBS at 4°C until SAXS radiation. For the CMTs fixed in relaxation buffer, CMTs were placed for 1h in growth media with varying concentrations of KCl relaxation buffer between 30 and 150 mM and then fixed in 4% PFA in growth media with the same concentration as before.

2.3 Sample Preparation for Synchrotron

For fixed tissue, biological data were recorded pre-fixation using an optical microscope equipped with a camera and contractions were recorded. Contractile force was measured based on the deflection of the PDMS pillars and their known measured stiffness (2.67 N/m)²⁴. Post fixation, the tissue was submerged in PBS to prevent desiccation, and was stored in a cold room at 4 °C until one day before transport to the synchrotron. 24 hours before transportation, excess PDMS was removed from the devices using a scalpel using a consistent method described below, and the isolated tissue on its PDMS platform was transferred to a new container, washed with PBS again, and placed back in the cold room.

To remove the excess PDMS from the well and PDMS that would otherwise block the SAXS beam, caution must be had in order to avoid any stress on the tissue as no adhesive is used to keep the tissue connected to the pillars. To do this, we developed a method consisting of a series of six cuts that that minimize mechanical stress placed on the tissue and the pillars. Three cuts are made parallel to the length of the tissue, close enough to separate the wall of PDMS from the block. The first two cuts are made on either side, with the third cut being used to fully separate the excess PDMS. Three more cuts are done on

the other side of the tissue. The last two cuts are made across the base of the well, touching the inside of the first wall of the well. This method of PDMS removal has a 70% success rate in removal of the PDMS while maintaining tissue connection to the pillars.

24 hours before measurements, the tissue was transported by a professional courier service to the synchrotron on ice and was kept on ice until SAXS measurements.

For live tissue, contractions were recorded and the excess PDMS was removed from the devices. The tissue was then submerged in fresh media that was regularly refreshed until the time of transportation and stored in an incubator at 37°C and 5% CO₂. For transportation, the tissue was transferred to an incubator (MyTemp Mini Digital Incubator h2200-h) that maintained the 37°C, 5% CO₂ environment. On the day of measurements, live tissue measurements were prioritized. All parameters of the SAXS setup remained the same between fixed and live tissue, except in live tissue measurements CMTs were irradiated for three seconds to cover a full contraction period.

2.4 SAXS Setup for Tissue Measurement

For SAXS measurement, the tissue samples remained stretched on the pillars of the PDMS platforms and, excess PDMS was removed to fit the sample in custom chambers constructed using a 70 μm -thick glass slide and Kapton tape. The tissues were submerged in room temperature PBS and the Kapton/glass chamber was attached to the SAXS sample holder for diffraction studies (Figure 8).

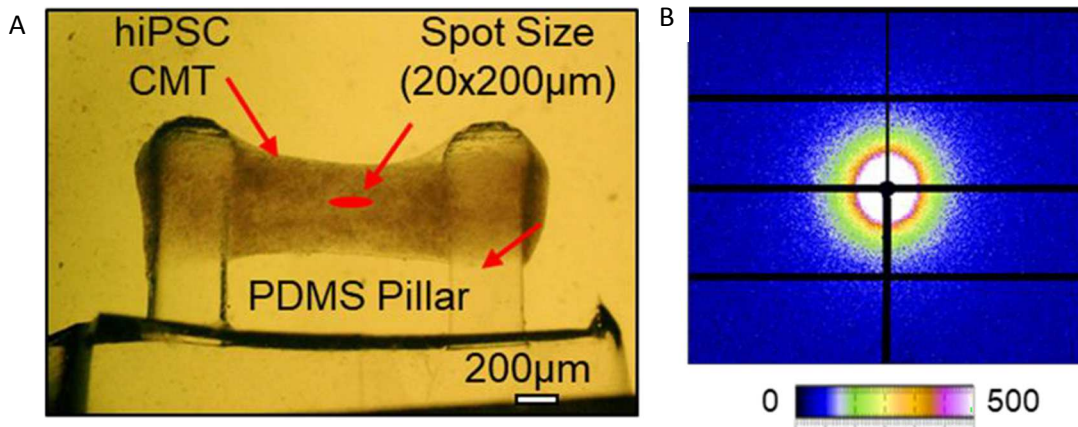


Figure 8: (a) Cardiac microtissue on pillars in Kapton-glass chamber. Samples are inverted in the chamber. (b) standard image result of x-ray diffraction¹⁹.

2.5 Data Acquisition

Because the samples being irradiated are organic material, it is generally advised to use a low x-ray energy. These studies employed either 14 keV

($\lambda=0.103$ nm) (batch 1) or 12 keV ($\lambda=0.00885$ nm) (batch 2 & 3). The detector used was a Pilatus3 X 1M and the sample-to-detector distance was 7.0 m. The flux was 1×10^{12} ph/s, the sample rate was 50Hz, and exposures time of 0.09s (batch 1) or 1s (batch 2 & 3) were used. The footprint of the x-ray beam on the tissue was $20 \mu\text{m} \times 200 \mu\text{m}$. These parameters resulted in a radiation dosage of 7.6 KGy (batch 1) and 72 KGy (batch 2). In both cases, the dose was well within the bounds of maximum allowable dosage determined in previous studies¹⁹. Background data was collected by sampling from sections near the tissue, but where there is only PBS in the chamber. For multiple measurements of the same tissue, a single background sample was collected.

SAXS measurements were collected using various experimental methods. For initial tests and live tissue tests, a single measurement was made in the center of the tissue. For the fixed tissue tests of batch 1, three measurements were made down a column (i.e., transverse to the long axis of the tissue), and for batch 3, nine measurements were taken on a 3x3 rectangular grid with a horizontal spacing of $200 \mu\text{m}$ and lateral spacing of $100 \mu\text{m}$.

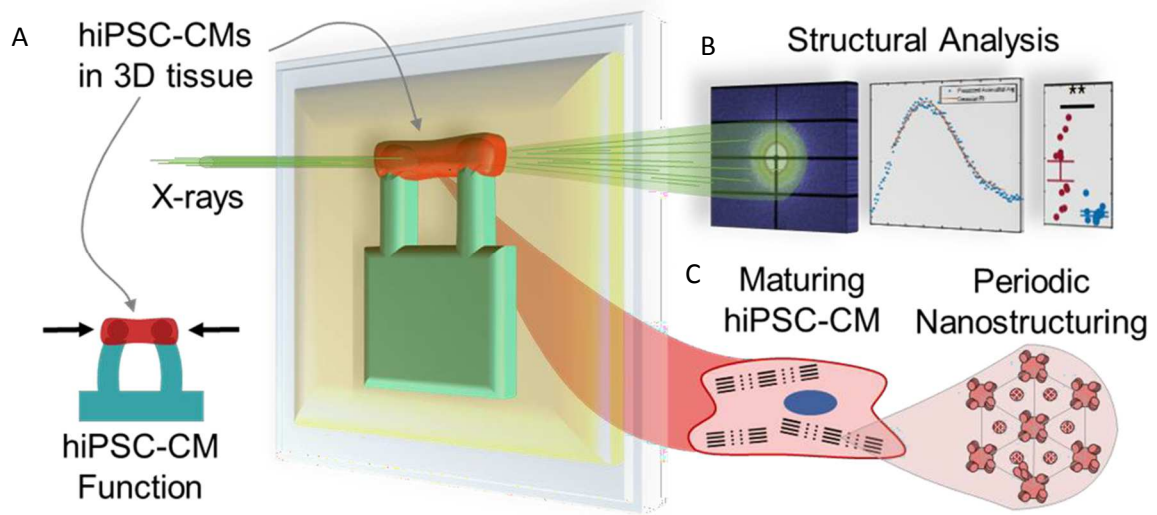


Figure 9: (a) Visual indicator of tissue orientation to SAXS beam and size of SAXS beam. (b) Standard TIF image result of SAXS measurement that is then converted into an intensity plot. (c) cardiomyocyte myoactin nanostructure¹⁹.

2.6 SAXS Data Python/MATLAB Processing and Analysis

The 2D diffraction obtained from the Pilatus detector were azimuthally integrated using pyFAI (python- Fast Azimuthal Integration) in a Jupyter Notebook environment²⁵. The workflow for data processing was originally developed by staff members at Brookhaven National Laboratory and modified and extended by Boston University students. Before azimuthal integration, the image is masked and filtered, eliminating outliers resulting from dead pixels, cosmic ray strikes, blank detector regions, and other artifacts. The collected background is also subtracted before integration. After integration, the data is

transformed into a Kratky plot, which plots Q^2I vs Q , to deemphasize the Q dependence of a featureless signal.

The diffraction of x-rays from planes of myosin and actin depends on the differing electron density in these planes and provides a direct measure of the myo-actin lattice order and spacing in the volume interrogated. The (1,0) plane is defined to be the lattice of the “thick” (myosin) filament (Figure 9). The SAXS scattering peak for the myofilament spacing will be approximately a wavenumber of $q = 0.145 \text{ nm}^{-1}$, associated with a 43 nm real space lattice dimension²⁰. To infer the position in q -space of the myofilament scattering peak, a linear regression is made further out from this signal around $q = 0.3 \text{ nm}^{-1}$, any signal from this region is due to noise or background and is outside our peak of interest. The linear regression is then subtracted from the signal. The myofilament scattering signal is assumed to have a normal distribution, so the data is therefore analyzed using a nonlinear fitting algorithm to determine the optimum Gaussian-function parameters. The model for the Gaussian fit provided information about the peak intensity, peak location, and full width at half maximum (FWHM). A typical FWHM in our measurement of cardiomyocytes is about 0.01 nm^{-1} . The location of the Gaussian peaks indicates the wavenumber associated with the mean spacing of the cardiomyocyte. This

spacing data is collected and imported for plotting in Microsoft Excel. MATLAB is used for ANOVA analysis to test for statistical significance, and the colormap function is used to create 2D interpolated colormaps of the spacing of the myofilament lattice as a function of position on the tissue.

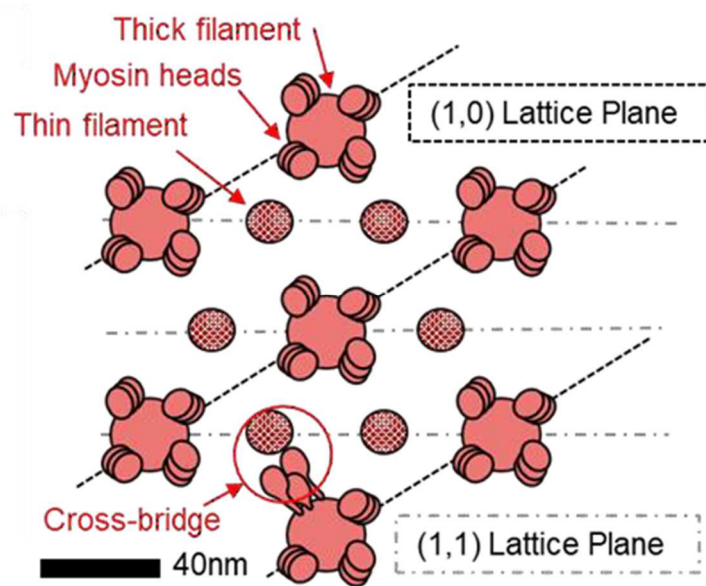


Figure 10: Visual of the 1,0 and 1,1 planes in the myo-actin complex¹⁹.

3 Results

3.1 Variance Based on Acquisition Method

By measuring the d-spacing of the myofilament lattice in multiple regions of the same tissue, averaged values are obtained for a given tissue that account for inconsistencies such as tissue deformation, intensity (SAXS beam imperfectly aligned with tissue), and general sample-to-sample variance in biological materials. In three separate experiments we tested three methods of data acquisition: first, a single measurement in the center of the tissue; second, three measurements down a column in the center of the tissue; and third, a 3x3 grid centered on the tissue. After averaging, the variance of the d-spacing between samples was significantly reduced, indicating that the spacing is very similar from sample to sample, but not necessarily in the same areas. Figure 11 shows the variance in the spacing vs acquisition method, with the 3x3 grid showing the lowest variance between samples.

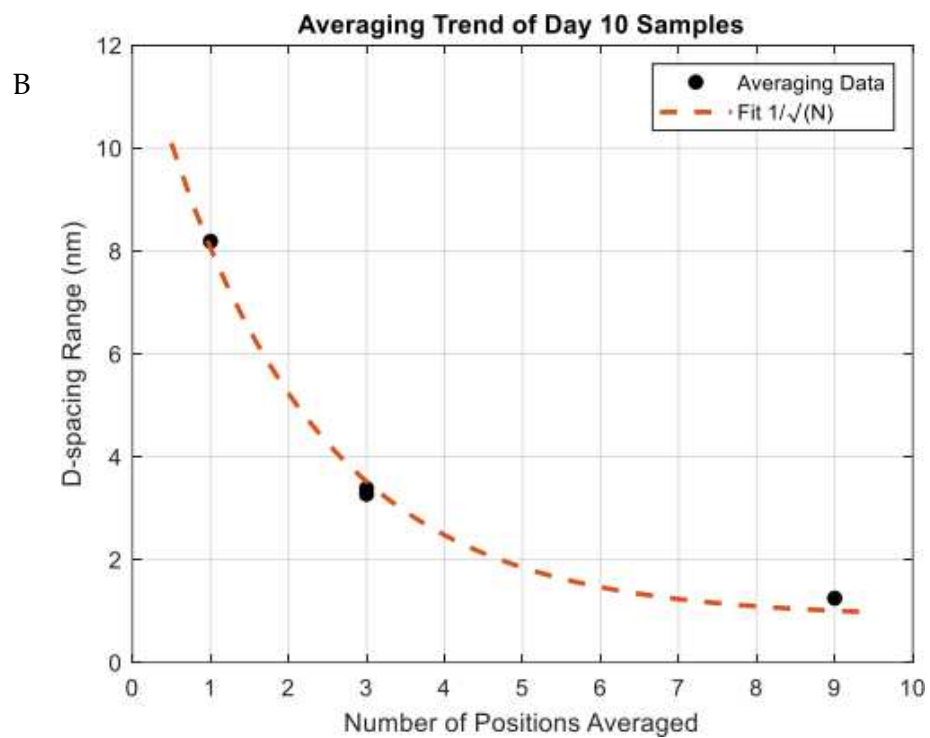
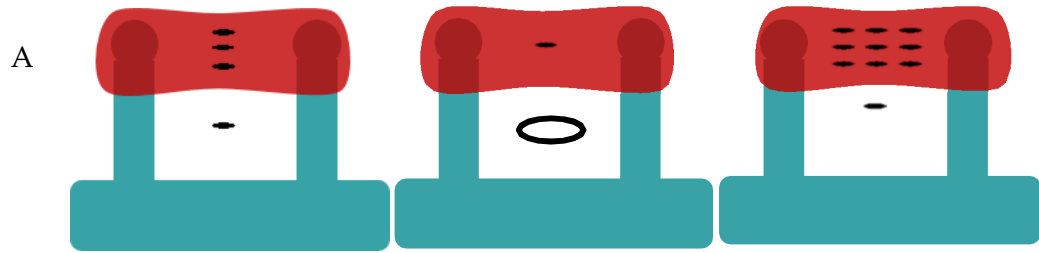


Figure 11: (A) Three tested methods for data collection in samples. Black bars indicate the approximate position of the SAXS beam. Bars outside tissue indicate collection of the background signal. For second method, background was not collected. Measurements were averaged to show overall spacing of tissue. (B) Plot of standard deviation of spacing of samples by number of points averaged. Method 3 covers majority of tissue and by averaging the measurements results in lowest variance.

3.2 Colormaps of Measurements

Figure 12A, below, presents a series of interpolated 2D colormaps showing the measured myofilament spacing of samples based on the position on the tissue. It was expected that the spacing would be generally lower at the extrema of the tissue where there is the most tensile stress on the cells. This is corroborated by significantly higher spacing observed in the center of tissue matured to Day 4. However, this finding is not observed in tissue that had matured for longer.

As the tissue matures, it is observed from these 2D colormaps that the myofilament spacing shows more signs of horizontal striations. This indicates higher uniformity in cellular organization in more matured tissue.

No definitive conclusions can be drawn from these colormaps due to incomplete data. However, the results show the value of collecting x-ray diffraction data at a dense grid of positions in cardiac tissue in order to observe unexpected spatial dependence of the structure.

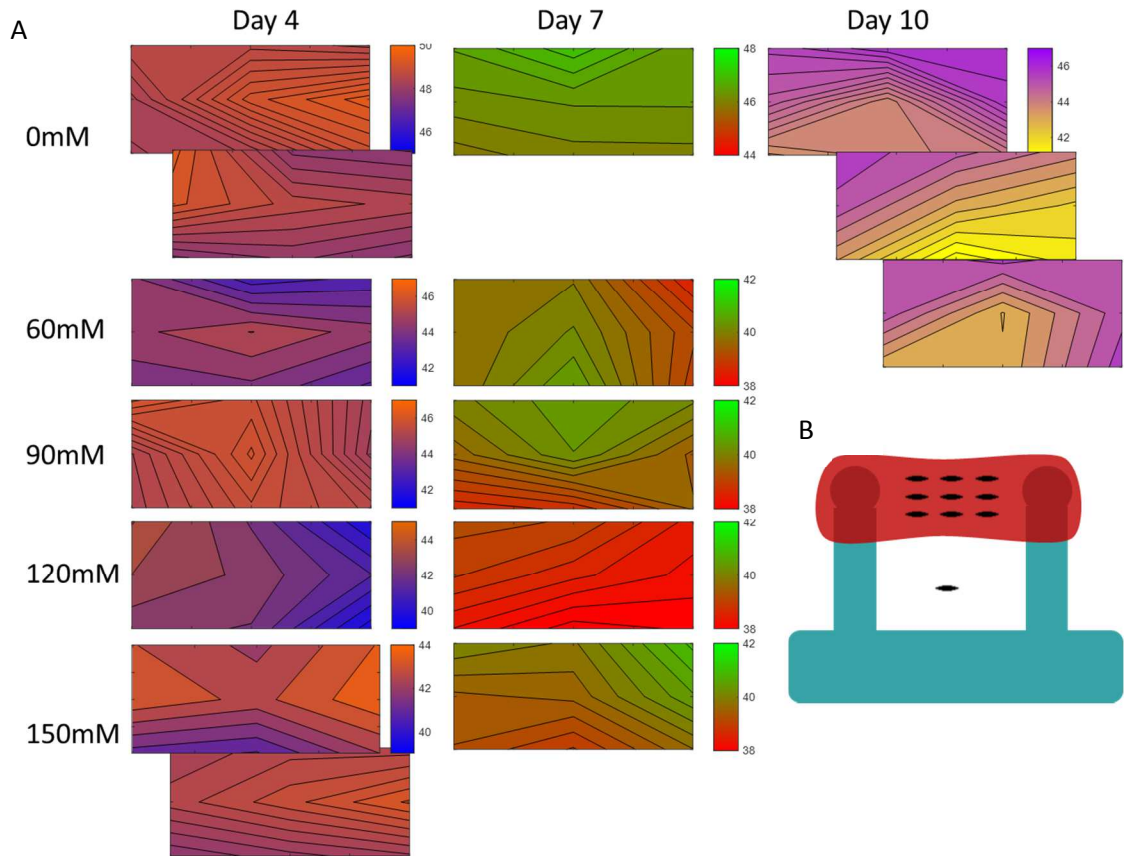


Figure 12: (a) Interpolated colormaps of the myofilament spacing in the tissue. Down column is maturation time of tissue. Rows indicate pre-exposure to varying conc. of relaxation buffer. Offset graphs indicate repeat measurements of separate tissue with same parameters. Maps without color bars are repeat measurements. (b) visual of location of SAXS measurements on tissue

3.3 D-Spacing vs. Maturation Time

The spacing of the myofilament lattice in newly seeded hiPSC-CMs was found to decrease at a rate of ~ 1 nanometer a day [Figure 13 A–C]. Tissue matured to Days 3–4 were measured to have a d-spacing in the range of 49–46 nm suggestive of a lack of time for development of cellular organization. By day 9–10, the myofilament d-spacing decreases to the 44–42 nm range, a trend that is

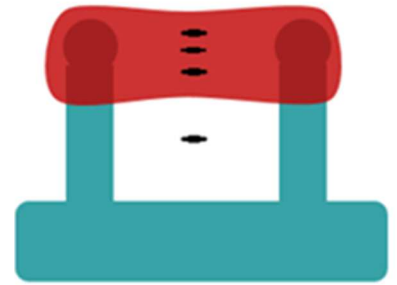
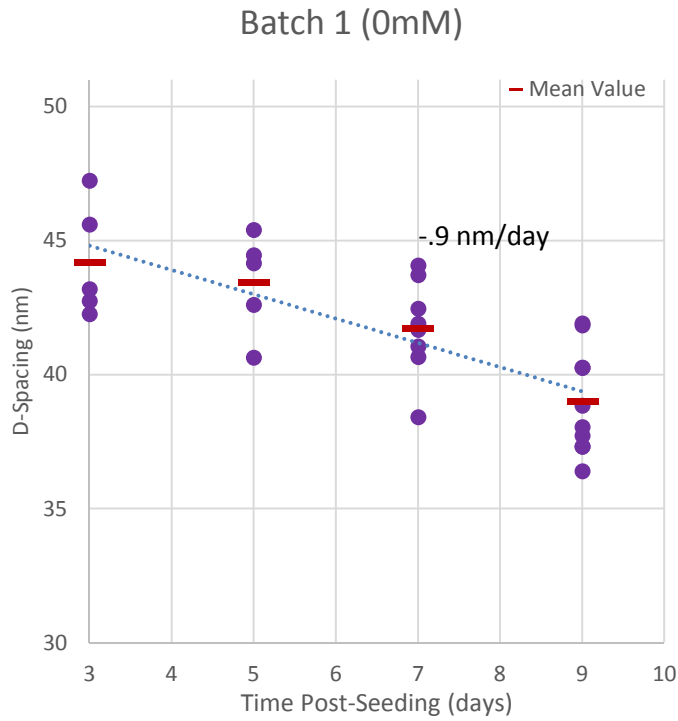
consistent with previous studies in myofilament spacing of hiPSC-CMs¹⁹.

ANOVA analysis of the myofilament spacing and maturation time results in a p value of 2.4×10^{-6} , denoting strong statistical significance. The average myofilament spacing did vary between experiments, however, 2-way ANOVA of the interaction term between batch and maturation time results in a p value of 0.92, denoting statistical insignificance. The trend of decreasing myofilament spacing with maturation time was consistent across experiments.

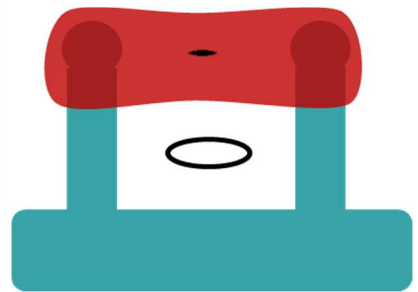
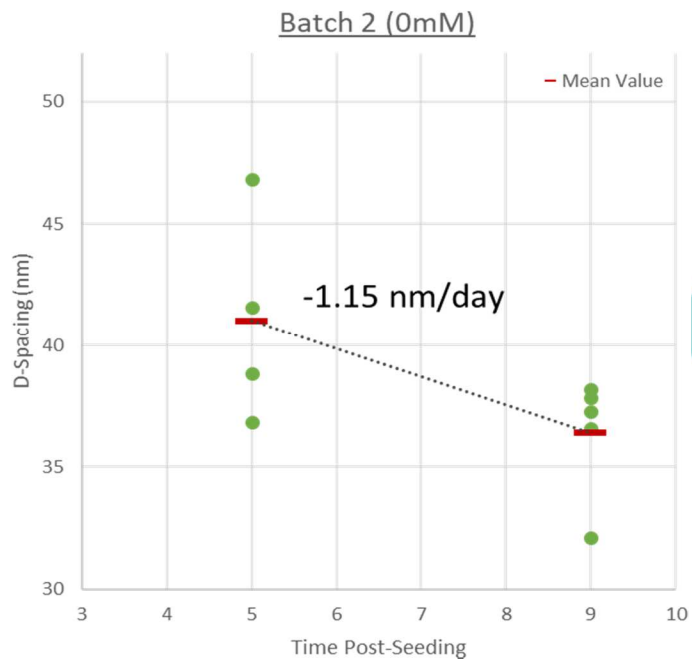
Measurements of tissue affected by the R403Q+ gene resulted in a similar trend of decreased spacing with increased maturation time. However, we have found that the lattice spacing of HCM tissue in the early stages of development is almost 5 nm greater than in wild type. The change in myofilament spacing of HCM tissue was also found to be 20% greater than in wild type [Figure 14].

The spacing of the myofilament lattice in bio-engineered hiPSC-CMs clearly changes over the first ten days of maturation after seeding. Adult cardiac muscle has previously been reported to be 39 nm.³ After ten days of maturation, the tissue measured in this study had a spacing of 43 nm. This is indicative of the structural differences between matured adult cardiac tissue and immature bioengineered hiPSC-CMs.

A



B



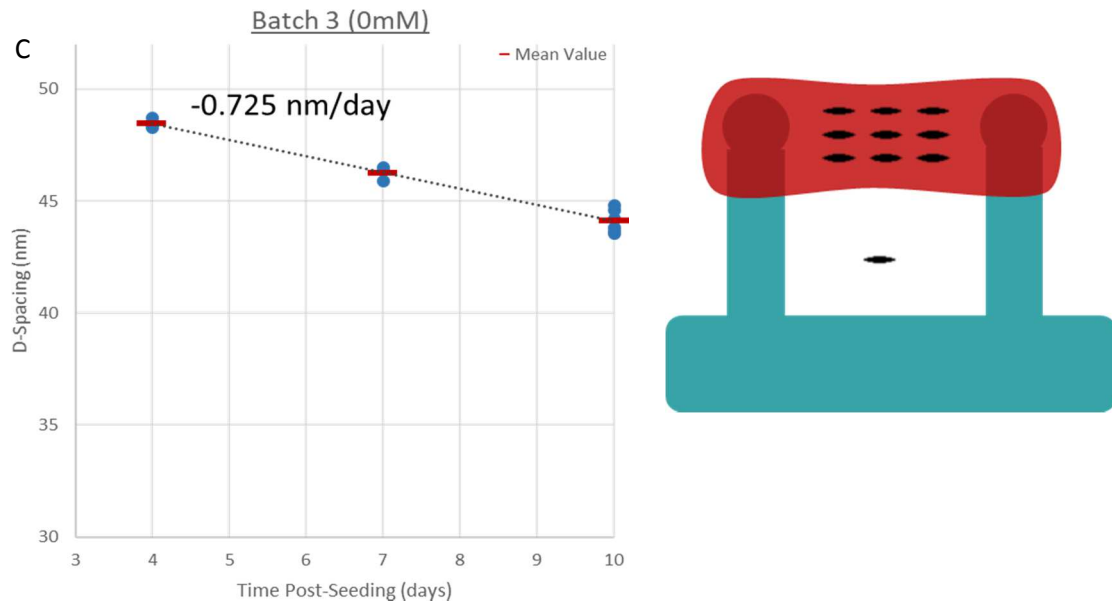


Figure 13: (A) *d*-spacing of myofilament vs maturation time for batch 1. Rate of change of -0.75 nm/day [N=27]. Visual of SAXS measurements taken in batch 1. (B) *d*-spacing of myofilament vs maturation time for batch 2, rate of change of -1.15 nm/day [N=19]. Visual of SAXS measurements taken in batch 2. (C) *d*-spacing of myofilament vs maturation time for batch 3. Rate of change of -0.725 nm/day [N=13]. Visual of SAXS measurements taken in batch 3.

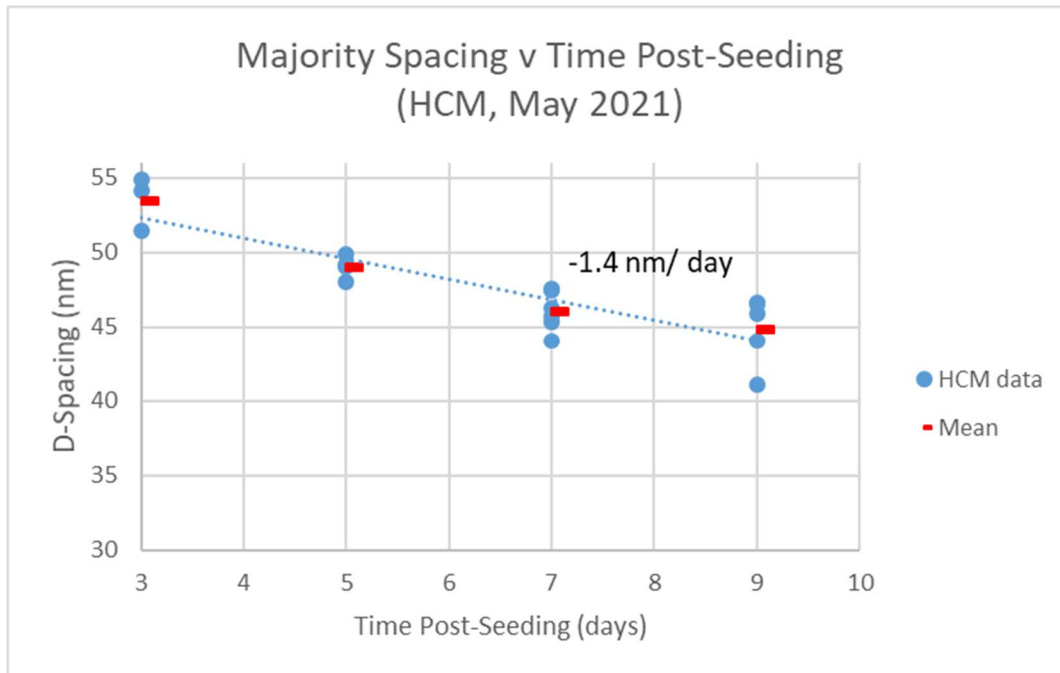


Figure 14: *d*-spacing of myofilament vs maturation time for HCM tissue as part of batch 1. Rate of change was -1.4 nm/day .

3.4 D-spacing Effect of Buffer

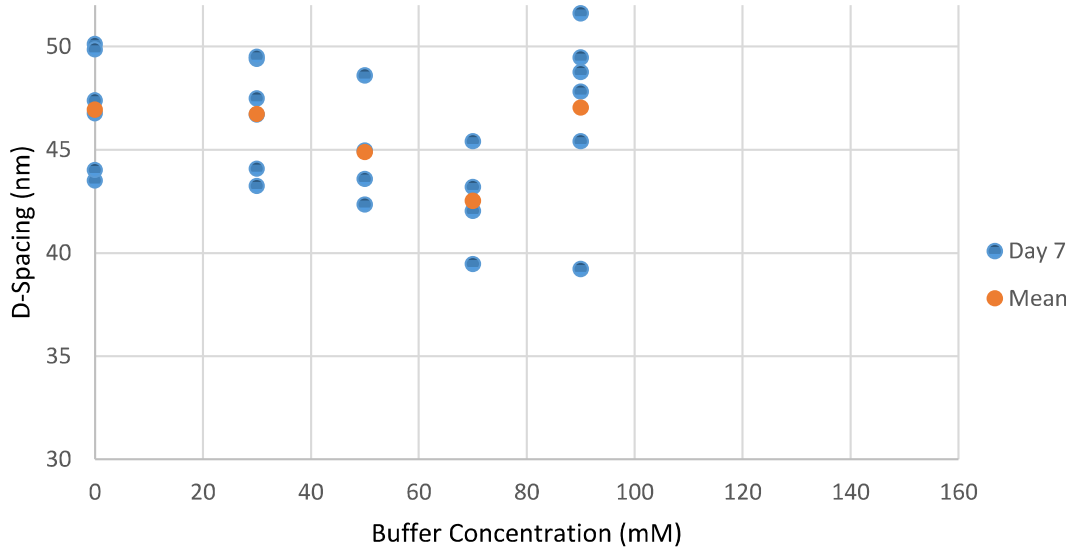
For our experiments exploring *d*-spacing as a function of maturation time, the tissue was fixed with formaldehyde and not treated with relaxation buffer. However, the concentration of the relaxation buffer the tissue was exposed to before fixation significantly impacts the spacing of the myofilament lattice. Tissue treated, before fixation, with increase concentration of KCl relaxation buffer showed reduced myofilament spacing [Figure 14], contrary to the expected trend.

In our first batch, we tested KCl concentration regions between 0 and 90mM. From 0 to 70mM, the myofilament spacing showed a non-monotonic decrease as a function of buffer concentration. This trend in the lower concentration region is mirrored in the measurements of our second batch; although measurements between 0 and 60mM were omitted, a similar decrease in spacing was observed. Between 60 and 90mM in the first batch there is a suggested increase in the myofilament spacing that is mirrored in the day 4 series of the second batch, but not in the day 7 series. Testing in higher concentration regions shows that for the day 4 series, this increase continues up to 120mM. This is then followed by a sharp decrease at 150mM that is consistent with the day 7 series again.

ANOVA analysis of this trend was not feasible because the data does not meet the criteria for valid ANOVA analysis. The sample size for this study was too small, so further studies with repeated measurements are needed in order to draw definitive conclusions.

A

D-Spacing vs Buffer Concentration (May 2021)



D-Spacing vs Buffer Concentration (July 2022)

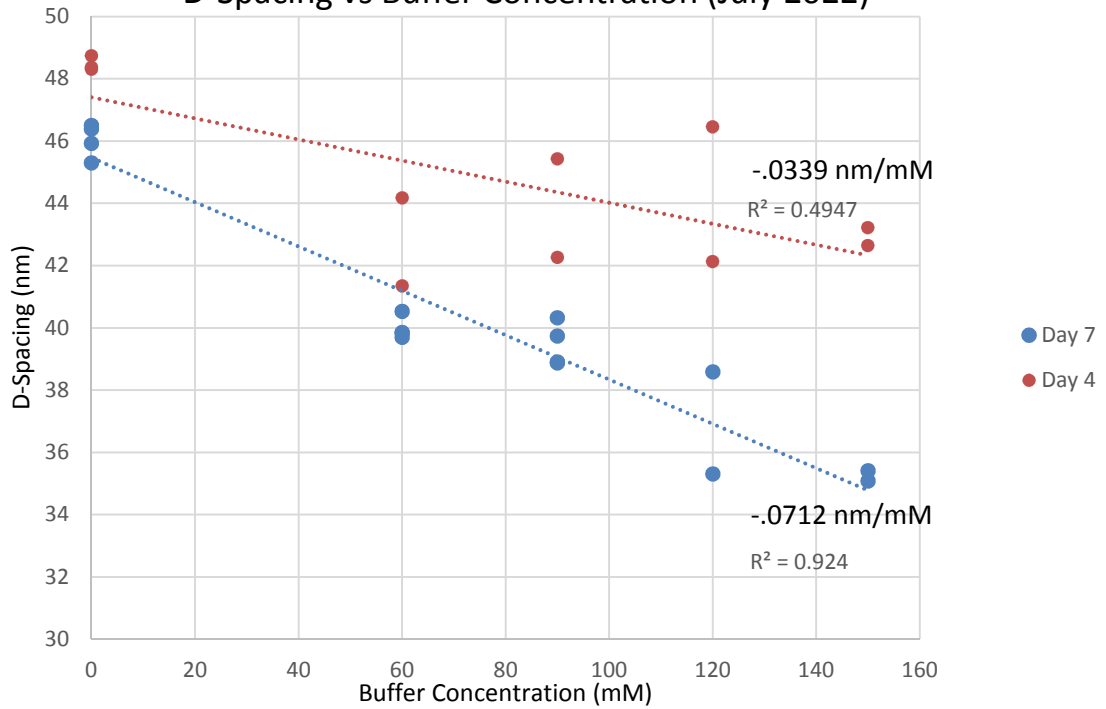
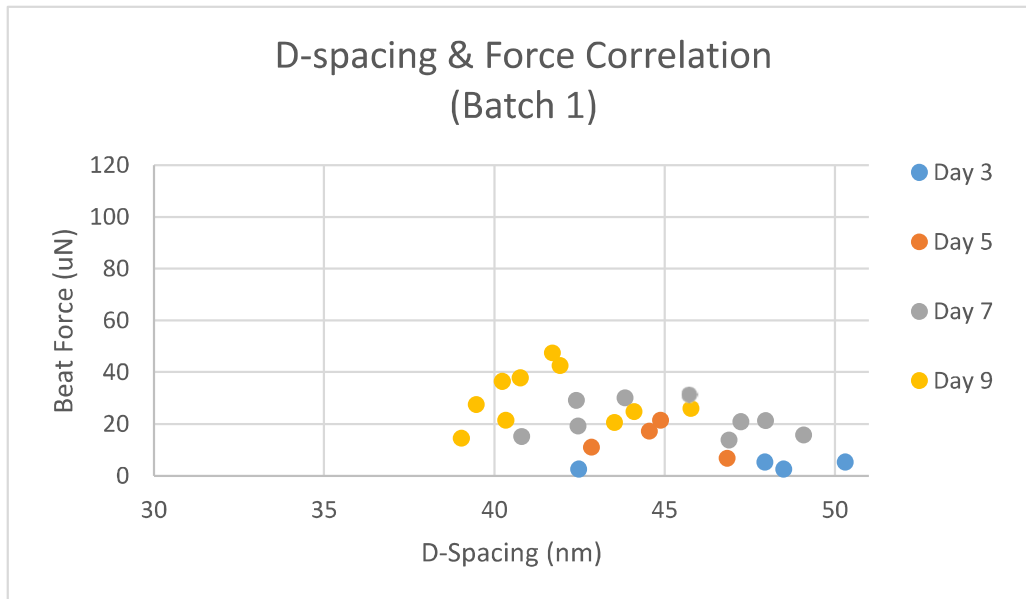


Figure 15: Myofilament d-spacing vs. concentration of KCl buffer for batches 1 (A) and 3 (B).

3.5 Structure Function Relationship

Video footage of the tissue contracting was recorded pre-fixation. An original MATLAB code developed by the Bishop lab was used to track the deflection of the PDMS pillar as the tissue contracted. This bending of the pillar was then used to calculate a crude indicator of the beat force of the tissue. Figure 16 below shows the beat force of the tissue pre-fixation plotted against the myofilament d-spacing. ANOVA analysis of the two variables resulted in a p value of 0.35 denoting statistical insignificance. The range of beat forces between the two batches should be noted, emphasizing the imprecision of this system.

A



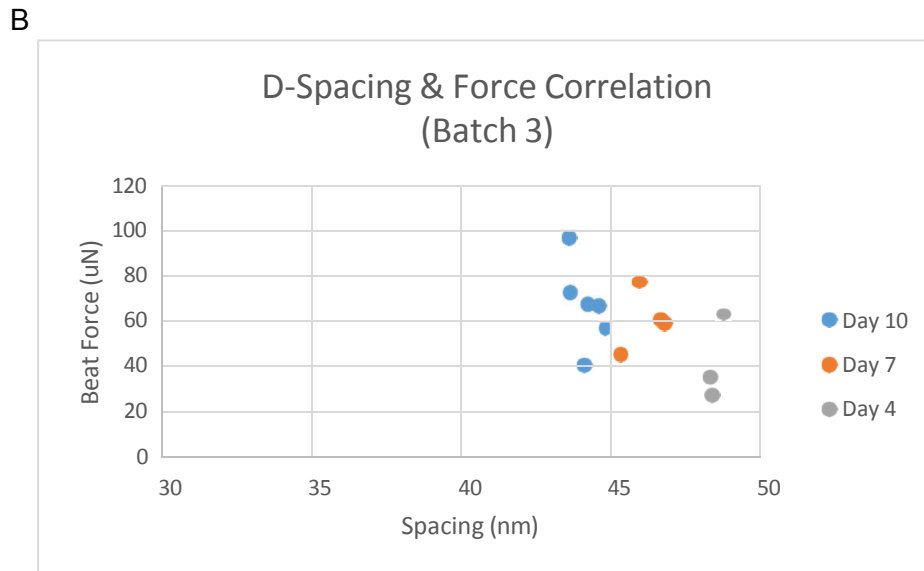


Figure 16: Beat force vs myofilament spacing for batches 1(A) and 3 (B).

3.6 SAXS LIVE TESTS

While this research focuses on the use of SAXS to study fixed tissue, in our experiments we made multiple attempts to use X-ray diffraction to monitor the nanostructure of engineered heart tissue during a live contraction. We did this by measuring tissue confirmed to be contracting with SAXS over an extended period of time. The majority of samples were observed to have an average contraction period of 1.5s [Figure 17], tissue data was collected for 3s with a sample rate of 50Hz. The spacing as a function of time was then plotted in Figure 18. The lattice spacing is observed to decrease by 2 nm over the measurement

time, going from 41.5 nm to 39.5 nm, with a slight increase at the end.

Measurements were taken in the approximate center of the tissue.

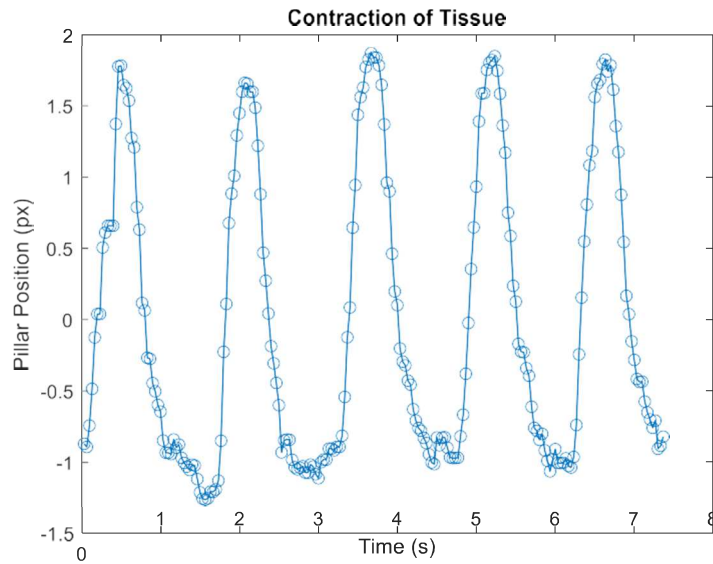


Figure 17: tracking results of movement of pillar that monitors contraction frequency and beat force

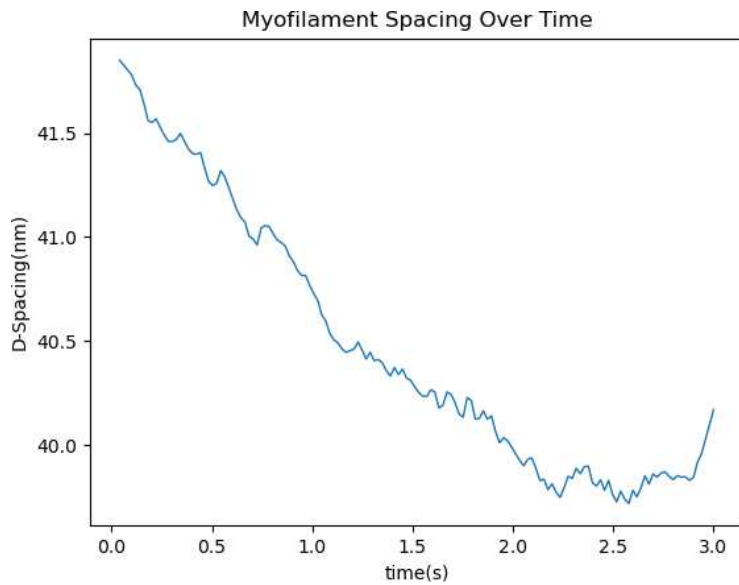


Figure 18: change in myofilament spacing over 3s of SAXS irradiation. No real indication of oscillation

4 Discussion

4.1 Spacing of the Myofilament lattice

To study structure function relationships in cardiac tissue, a consistent and effective method of imaging is required to be able to characterize the nanostructure and connect it to other biological measurements. Most imaging methods are incapable of resolution at the nanometer scale and those that are suffer from an inability to measure the structure without causing severe damage to the tissue. SAXS measurements combined with reliable methods of data acquisition and processing are capable of consistent measurements of the myofilament lattice with decent signal-to-noise ratio.

The grid style measurement employed in this work is highly beneficial as it is the first map of the myofilament spacing in a hiPSC-CM sample using SAXS. Through this 3D characterization we can monitor changes in the uniformity of the spacing in the cardiac tissue as it matures and determine whether cellular organization occurs universally or not. We observed higher spacing in the center of the tissue matured to day 4 as compared to the periphery, a distinction not observed in tissue matured past day 7. There is a possibility that environmental factors can affect the spacing of the tissue and this effect will be most observable

at the tissue's extrema. The lack of this distinction in matured tissue implies a prioritization of cellular organization in the tissue. Furthermore, we specifically observed a greater degree of horizontal striations in the most matured tissue, indicating a higher level of ordering. This mapping method can be used to test the effect of mechanical stress on the d-spacing as well as further studies on anisotropy of tissue that is cultivated this way, *in vitro*, as described in the Methods section.

Many factors affect the cellular structure of biological materials, and while some are understood and well-characterized, others have not been fully characterized, are incompletely understood. Since we cannot control for unknown confounding factors, this can lead to large sample-to-sample variance in structural measurements of tissue. However, while the uncertainty may be large for measurements at a specific position in a tissue, the combined measurements suggest an overall structure with little sample to sample variance [Figure 11B]. By measuring the tissue in a grid of positions and interpreting the collection of measurements, we can draw firm conclusions about the overall structure of a tissue, rather than in a highly localized position. This work enables us to conclude the myofilament spacing of immature hiPSC-CMs to be within a certain variance (± 2 nm), much smaller than previous measurements were able

to identify (± 6 nm). We also conclude that this range changes as a function of maturation time. The myofilament spacing is shown to decrease with time, with tissue that has matured for three days showing an average spacing of 48 nm and after 7 days this spacing has decreased to 45 nm (significant at $p < .05$). Different batches yielded absolute spacings that were different on days 3 and 10; however, the *change* in spacing was consistent within a standard deviation of ± 0.2 nm/day. This suggests a universal rate for development of organization in these CMTs. Interestingly, while the spacing in the hypertrophic (HCM) tissue in the earlier stages of maturation was observed to be over 20% greater, the HCMs showed similar spacing to the wild-type tissue in its development at day 9; however, the rate of development was significantly higher at 1.4 nm/day, suggesting that with further time for structural development, the cardiac myofilament spacing does not mirror what is seen in wild type. This difference is likely caused by the genetic mutation, which causes heart tissue to thicken and become denser. Knowledge of this developmental difference in HCM tissue could lead to the development of new therapies to reduce the likelihood of cardiac arrest in patients.

4.2 Effect of relaxation buffer on the d-spacing

The equilibrium concentration of potassium ions $[K^+]$ in a cardiomyocyte is extremely important in the regulation of the membrane potential. KCl by itself can be used to hyperpolarize the membrane potential, preventing the uptake of Ca^{2+} , and thereby reducing the likelihood of a contraction. Shifts in this concentration can create cascade effects involving other ion channels and possibly affecting the uptake of Ca^{2+} and thus the action potential of the cell²⁶.

There is, however, no widely accepted expectation that KCl as a relaxation buffer affects the subcellular structure of cardiomyocytes. Some studies have theorized that the subcellular structure can be affected by changes in the diastolic volume of the cell induced by chemical equilibrium changes. By influencing the extracellular concentration of $[K^+]$, the cell will swell to rebalance the intracellular concentration and this cell volume change has been found in some studies to cause changes in the interfilament spacing of the cardiac myo-actin lattice²⁷.

While this presents an explanation for cellular physical changes induced by KCl, there is little consistent evidence of this fact, and indeed, this does not fully correlate with our findings.

In our experiments studying the effect of KCl buffer concentrations on the thick filament lattice spacing, we consistently observed notable changes in the myofilament structure as a function of extracellular KCl. These changes, however, are not monotonic nor consistent across different experimental groups. The structural change in response to [KCl] was nearly two times greater in Day 7 tissue as it was in Day 4 tissue. In low concentrations ($< 60\text{mM}$), KCl was shown to decrease the spacing of the myofilament lattice. This trend appeared to reverse in mid-concentration regions for day 4 CMTs ($60\text{mM} < [\text{KCl}] < 120\text{mM}$), that is, the d-spacing increased with concentration. However, this was not the case for the day 7 tissues in batch 3. Finally, with higher concentrations of KCl relaxation buffer (120mM), the spacing continued to decrease with concentration. This may reflect the balance between intra- and extracellular [KCl].

4.3 Contractility of hiPSC-CMs

This study characterized the structure of engineered cardiomyocytes and explored the relations between structure and function. Complete understanding of this relationship can inform cultivation methods of hiPSC-CMs that more closely simulate the capabilities of matured heart tissue. To that end,

characterizing the relationship between the beat force and the myofilament lattice structure is important.

The contractility of bio-engineered cardiomyocytes is generally lower than that of matured animal heart tissue. Despite this, we found the relationship between structure and function observed in this study is consistent with previous studies on the relationship between interfilament spacing and contractility, as seen in figures 15 and 16. It has been shown previously that reduction in the interfilament distance results in increased force generation within a cardiomyocyte¹⁵. Graphically it can be observed that beat force decreases with increased spacing. ANOVA analysis of our collected data determined this relationship to be statistically insignificant, however, the disparity on visual examination in the beat force between lower d-spacing and higher d-spacing is suggestive of consistency with previous studies. The lack of statistical significance is likely a result of the imprecision of the system due to a number of factors including time outside incubator, mechanical stress, growth around pillar, etc.

More data collection is needed to establish a statistically significant relation between increased beat force and spacing.

4.4 Contraction Tests

In our measurements of live contracting tissue, samples were observed to be beating before SAXS measurement as well as after. SAXS based determination of the myofilament spacing showed a 2 nm decrease in the first three seconds followed by a slight increase in the last second. Such nonmonotonic variation would be expected if the myofilament spacing varied with a contraction, but the period implied by SAXS measurements is not consistent with the shorter period observed visually. The sample is kept at high temperatures (37 °C) and is not chemically fixed. Therefore, the decrease in measured d-spacing may be an artifact due to sample drift during the measurement time frame. Similarly, a change in the spacing measurement could be due to a change in the orientation of the sample caused by movement.

While there may be structural changes within the myo-actin complex during a contraction, our preliminary experiments do not support the hypothesis that the spacing of the thick filament changes during a contraction. In future experiments measuring contractions, focus should be placed on induced contractions in relaxed tissue to more clearly correlate changes in the myofilament spacing with the stages of contraction. Constant monitoring of the

tissue during SAXS measurement is necessary in correlating a full contraction with a change in the d-spacing as well as observing any drift or changes to the orientation of the tissue.

5 Conclusion

This work has taken advantage of the tremendous ability of a synchrotron x-ray beam to be focused to a small footprint and 3 dimensionally characterize the signal of a subtle aspect of the nanostructure of cardiomyocytes with an adequate signal to noise ratio. Access to a state-of-the-art beamline is necessarily limited, but we were fortunate to be able to take advantage of the SAXS beamline at Brookhaven National Laboratory, in person, three times over the course of this research. Cultivation of cardiomyocyte tissue inevitably includes the possibility of unexpected mishaps, including in the transportation and preparation of delicate tissue to the facility. These factors limited the sample size and sample distribution, but successive improvements in techniques and methods allowed robust findings to be reported.

For example, we developed a novel and relatively effective technique for removing the tissue from the PDMS platforms, as described in the Materials and Methods Section. We also identified a method for SAXS data acquisition that generates improved accuracy of the measurements of the tissue after averaging, and which also provides 3D characterization of the tissue. In future experiments, this method can be used to characterize the subcellular nanostructure of hiPSC-CMs in a variety of different ways, including:

- understanding the relationship between mechanical stress and filament spacing
- characterizing and understanding the role of maturation and anisotropy
- determining the role of KCl (or other relaxants/contractants) buffer concentration on the uniformity/filament spacing.

Furthermore, all of these possibilities are relevant not only to fixed wild type tissue, but also to live tissue and to HCM tissue. Improvement in the overall SNR of the measurements is necessary for the development of this form of bio-imaging. In future experiments, comparison should be made between unaltered and demembrated tissue to characterize the impact of macromolecular components on the SNR of SAXS measurements.

Understanding the structural difference between matured adult human tissue and immature hypertrophic CMs is the key to unlocking therapies and better systems for growing bioengineered hiPSC-CMs that can function like and model naturally derived cardiomyocytes.

References

1. The top 10 causes of death. <https://www.who.int/news-room/fact-sheets/detail/the-top-10-causes-of-death>.
2. Nguyen, A. H. *et al.* Cardiac tissue engineering: state-of-the-art methods and outlook. *Journal of Biological Engineering* **13**, 57 (2019).
3. Bielawski, K. S., Leonard, A., Bhandari, S., Murry, C. E. & Sniadecki, N. J. Real-Time Force and Frequency Analysis of Engineered Human Heart Tissue Derived from Induced Pluripotent Stem Cells Using Magnetic Sensing. *Tissue Engineering. Part C, Methods* **22**, 932–940 (2016).
4. Rotenberg, M. *et al.* Silicon Nanowires for Intracellular Optical Interrogation with Sub-Cellular Resolution. (2019). bioRxiv doi:10.1101/825489.
5. Kuhn, E. R. *et al.* Nanothermometry Reveals Calcium-Induced Remodeling of Myosin. *Nano Letters* **18**, 7021–7029 (2018).
6. Moss, R. L. & Fitzsimons, D. P. Frank-Starling Relationship. *Circulation Research* **90**, 11–13 (2002).
7. actin | Definition & Function | Britannica.
<https://www.britannica.com/science/actin>.
8. Solaro, R. J. Mechanisms of the Frank-Starling Law of the Heart: The Beat Goes On. *Biophysical Journal* **93**, 4095–4096 (2007).

9. P., P., Shanmugam, L. & Prasath, P. A review of role of lung ultrasound and clinical congestion score in acute left ventricular failure. *International Journal of Advances in Medicine* **7**, 720 (2020).
10. Olsson, G. Reticles. in *Encyclopedia of Optical and Photonic Engineering (Print) - Five Volume Set* (CRC Press, 2015).
11. Poole, J. J. A. & Mostaçõ-Guidolin, L. B. Optical Microscopy and the Extracellular Matrix Structure: A Review. *Cells* **10**, 1760 (2021).
12. Denk, W., Strickler, J. H. & Webb, W. W. Two-Photon Laser Scanning Fluorescence Microscopy. *Science* **248**, 73–76 (1990).
13. Bub, G. *et al.* Measurement and analysis of sarcomere length in rat cardiomyocytes in situ and in vitro. *American Journal of Physiology. Heart and Circulatory Physiology*. **298**, H1616–H1625 (2010).
14. Mielańczyk, Ł. *et al.* Transmission Electron Microscopy of Biological Samples. In K. Maaz (ed.) *The Transmission Electron Microscope - Theory and Applications* (IntechOpen, 2015). doi:10.5772/60680.
15. Shen, J. *et al.* Effect of venovenous extracorporeal membrane oxygenation on the heart in a healthy piglet model. *Journal of Cardiothoracic Surgery* **8**, 163 (2013). <https://doi.org/10.1186/1749-8090-8-163>

16. What is small angle X-ray scattering (SAXS) - BIOSAXS GmbH.
<https://www.biosaxs.com/technique.html>
17. Nielsen, S., Gillilan, R. & Ando, N. Synchrotron-based small-angle X-ray scattering of proteins in solution. *Nature Protocols* **9**, 1727–1739 (2014).
18. Brunello, E. *et al.* Myosin filament-based regulation of the dynamics of contraction in heart muscle. *Proceedings of the National Academy of Sciences of the United States of America* **117**, 8177–8186 (2020).
19. Javor, J. *et al.* Probing the subcellular nanostructure of engineered human cardiomyocytes in 3D tissue. *Microsystems & Nanoengineering* **7**, 1–8 (2021).
20. Nicolas, J.-D. *et al.* X-ray diffraction imaging of cardiac cells and tissue. *Progress in Biophysics and Molecular Biology* **144**, 151–165 (2019).
21. Toepfer, C. N. *et al.* Myosin Sequestration Regulates Sarcomere Function, Cardiomyocyte Energetics, and Metabolism, Informing the Pathogenesis of Hypertrophic Cardiomyopathy. *Circulation* **141**, 828–842 (2020).
22. Lian, X. *et al.* Directed cardiomyocyte differentiation from human pluripotent stem cells by modulating Wnt/ β -catenin signaling under fully defined conditions. *Nature Protocols* **8**, 162–175 (2013).
23. Javor, J., Sundaram, S., Chen, C. S. & Bishop, D. J. A Microtissue Platform to Simultaneously Actuate and Detect Mechanical Forces via Non-Contact

- Magnetic Approach. *Journal of Microelectromechanical Systems* **30**, 96–104 (2021).
24. Legant, W. R. *et al.* Microfabricated tissue gauges to measure and manipulate forces from 3D microtissues. *Proceedings of the National Academy of Sciences of the United States of America* **106**, 10097–10102 (2009).
 25. General introduction — pyFAI 0.22.0a10 documentation.
<https://pyfai.readthedocs.io/en/master/pyFAI.html>.
 26. Conduction System Tutorial. <http://www.vhlab.umn.edu/atlas/conduction-system-tutorial/cardiac-action-potentials.shtml>.
 27. April, E. W. & Brandt, P. W. The Myofilament Lattice: Studies on Isolated Fibers : III. The effect of myofilament spacing upon tension. *Journal of General Physiology* **61**, 490–508 (1973).

CURRICULUM VITAE

